Special issue on Mixed Mode Fracture
Theoretical and Applied Fracture Mechanics – January 2017
REVISED VERSION - February 2017

Mode I fracture toughness of fibre reinforced concrete

Andrea CARPINTERI, Giovanni Fortese, Camilla RONCHEI, Daniela SCORZA, Sabrina VANTADORI

Dept. of Engineering and Architecture,
University of Parma, Parco Area delle Scienze 181/A, 43124 Parma, Italy
Corresponding Author: Sabrina Vantadori sabrina.vantadori@unipr.it

ABSTRACT

Low fracture toughness of concrete represents a serious shortcoming. An effective way to improve the concrete toughness is represented by the dispersion (during mixing) of discontinuous fibres into the concrete mix. The principal beneficial effect of fibres is the crack bridging in the cementitious matrix, providing resistance to crack propagation before fibre debonding and/or pulling out or failure. In the present paper, the fracture behaviour of FRC (fibre reinforced concrete) specimens is examined, with micro-synthetic polypropylene fibrillated fibres being randomly distributed in concrete. The modified two-parameter model, proposed by the authors to calculate Mode I plain-stain fracture toughness for quasi-brittle material, is able to take into account the possible crack deflection (kinked crack) during stable crack propagation.

KEYWORDS: Fibre reinforced concrete, fracture toughness, micro-synthetic polypropylene fibrillated FRC, modified two-parameter fracture model

NOMENCLATURE

$\underline{a}$	effective critical crack length
a_0	notch length
a_1, a_2	kinking crack length
B	specimen thickness
C_i	initial compliance
C_u	unloading compliance
E	elastic modulus
I_e	error index
K_{IC}^S	Mode I critical stress-intensity factor
$K_{(I+II)C}^S$	mixed mode critical stress-intensity factor
$P_{\max}$	peak load
S	specimen loading span
W	specimen depth

$\alpha_0 = a_0 / W$	initial notch-depth ratio
$\alpha = \underline{a} / W$	effective notch-depth ratio
θ	kinking crack angle

ACRONYMS LIST

CCM	cohesive crack model
CBM	crack band model
CMOD	crack mouth opening displacement
DKFM	double-K fracture model

ECM	effective crack model
FRC	fibre reinforced concrete
FPZ	fracture process zone
LEFM	Linear Elastic Fracture Mechanics
MTPM	modified two-parameter model
NEFM	Nonlinear Elastic Fracture Mechanics
SEM	size effect model
TPFM	two-parameter fracture model

1. INTRODUCTION

Concrete is extensively used as construction material in the civil engineering practice due to: (i) low production costs, (ii) easiness to be cast in different shapes, and (iii) versatility in response to different design requirements [1,2].

Despite its several merits, concrete has low tensile strength and weak cracking resistance. Fracture toughness, which represents the cracking resistance capability, is a fundamental parameter to analyse the fracture behaviour of concrete [3].

As is well-known, concrete needs a fracture mechanics approach different from that for metals [4]. For both metallic and concrete structures, fracture mechanics is nonlinear due to the presence of a zone ahead of stress-free crack tip, where the material shows a nonlinear behaviour [4]. Such a zone is named plastic zone in ductile and brittle metals and is mainly characterised by either hardening plasticity or perfect yielding of the materials, whereas such a zone is named fracture process zone (FPZ) in concrete and

undergoes a softening damage (tearing). Concrete, as well as rocks and many other materials, are commonly named quasi-brittle materials.

In ductile metals, the applied energy is dissipated as plastic energy to form plastic zones [2,5,6], and Nonlinear Elastic Fracture Mechanics (NEFM) can be employed to examine fracture behaviour. In brittle metals, the applied energy is consumed as surface energy to form new crack surfaces [2,7], with the surface energy being significantly greater than the plastic energy, and Linear Elastic Fracture Mechanics (LEFM) can be applied to analyse the fracture process and crack propagation. In quasi-brittle materials, energy is used to form the fracture process zone [2].

Until early 1970s, many investigations were aimed at the application of LEFM in order to examine fracture process and crack propagation [8]. On the basis of such studies, it was well established that LEFM can be employed to large-scale concrete structures only, whereas it cannot be applied to medium/small-mass structures due to the presence of large FPZs [8]. Since late 1970s, starting with the pioneering work by Kaplan [9], concrete fracture has been a subject of great interest.

Many nonlinear fracture models have been proposed by several research groups to study the fracture behaviour of concrete, both to take into account the effect produced by FPZ on concrete nonlinear fracture behaviour and to implement the governing mechanisms in nonlinear fracture [3]. The fundamental fracture models are: the cohesive crack model (CCM) [10], the crack band model (CBM) [11], the two-parameter fracture model (TPFM) [12], the size effect model

(SEM) [13,14], the effective crack model (ECM) [15-18] and the double-K fracture model (DKFM) [19-22]. Recent significant proposals are available in the literature [23-25].

For both TPFM and SEM, RILEM recommended the guidelines for the determination of fracture toughness [26-29]. RILEM also recommended the guidelines to determine fracture energy by means of three-point bending tests performed on notched specimens [30].

As has previously been mentioned, concrete is characterized by low fracture toughness [31]. The fracture failure at the microscope scale, irrespective of the external applied loading, is produced by local concentration of tensile stresses and strains near defects. Low fracture toughness represents a serious shortcoming. An effective way to improve the concrete toughness is represented by the dispersion, during mixing, of discontinuous fibres into the concrete mix [32].

The principal beneficial effect of fibres appears after cracking of the matrix [33]: as a matter of fact, by bridging cracks in the matrix, they provide resistance to crack propagation before fibre debonding or pulling out or failure [1]. Further, fibres are able to reduce both shrinkage and shrinkage cracking, related to curing and hardening of concrete.

Since different orders of magnitude in FRC fracture energy with respect to plain concrete one are commonly observed [34-37], possible applications of FRC include buildings, highway overlays, bridges, airport runways [34-36] and explosion and shock resistant structures [33].

Fibre bridging is responsible for high energy absorption. Many tests have been proposed to measure such an energy absorption capacity [38]. The flexural test, able to realistically simulate the conditions in many practical applications, has commonly been used [38] according to standards, recommendations and other significant proposals available in the literature, as was reviewed by Gopalaratnam et al. in Refs [38,39]. Further, other interesting proposals have been published [40-46].

Moreover, the application of nonlinear fracture models presented for plain concrete has also been extended to FRC [47-49]. Note that the application of ECM is not possible, since it characterises the matrix-dominating response only [50].

In such a contest, a method proposed by the present authors to calculate the Mode I plain-stain fracture toughness for quasi-brittle material [51] is employed. It follows the same framework of the TPFM [12], that is: a three-point bending test on a single-notched specimen is performed; then the registration of the applied load against the crack mouth opening displacement (CMOD) and the expressions related to a crack loaded in Mode I are used to compute the fracture toughness (i.e. the critical stress-intensity factor).

The novelty of such a model, named the modified two-parameter model (MTPM), with respect to the TPFM is that the MTPM is able to take into account the possible crack deflection (kinked crack) during stable crack propagation. As a matter of fact, fracture toughness would be overestimated by considering crack propagation under pure Mode I loading (that is, by applying the TPFM). The MTPM, instead, allows us to take into account that cracks in FRC may

deflect during fracture extension, even in the case of a far-field Mode I loading, as is experimentally observed. Although the method is not predictive since the kinking angle value has to be measured through an experimental campaign, it allows us to determine a more realistic value of fracture toughness.

Such a deflection is caused by the biaxial stress state due to normal stress produced by bending, and shear stress produced by slippage at interface between cementitious matrix and fibre.

Testing is performed on FRC specimens, where micro-synthetic polypropylene fibrillated fibres (length=18mm, aspect ratio=0.003) are randomly distributed in concrete with different values (0.0, 0.5 and 2.5% by volume) of fibre volume fraction, called fibre content in the following. The fracture toughness is observed to improve by both adding fibres to concrete and increasing the fibre content.

2. MODIFIED TWO-PARAMETER MODEL

The modified two-Parameter model (MTPM) was proposed by the authors in Ref.[51] to compute the fracture toughness of quasi-brittle materials (for example, bone), when crack propagates under mixed mode loading (Mode I together with Mode II). Such a model can be also employed in the present study, FRC being a quasi-brittle behaviour.

According to the MTPM, the specimen has a prismatic shape and presents a notch in the lower part of the middle cross-section (Figure 1). As in the case of the TPFM [12], the following specimen sizes are employed: $W = 2B$ (where W and B are depth and width of

the specimen, respectively), notch-depth ratio $\alpha_0 = a_0/W = 1/3$, and loading-span/depth ratio = $S/W = 4$ (Figure 1).

Figure 1.

The tests are performed under three-point bending loading and crack mouth opening displacement control. More precisely, the specimen is monotonically loaded up to the peak load, P_{max} (Figure 2). When such a load value is achieved, the post-peak stage follows and, as soon as the force equals 95% of P_{max}, the specimen is fully unloaded (Figure 2). Then the specimen is reloaded up to failure.

Figure 2.

The linear elastic compliance C_i (named initial compliance) is used to determine the elastic modulus E [12,51]:

$$E = \frac{6 S\, a_0 V(\alpha_0)}{C_i W^2 B} \tag{1}$$

where parameter $V(\alpha_0)$ is given by [52]:

$$V(\alpha_0) = 0.76 - 2.28\alpha_0 + 3.87\alpha_0^2 - 2.04\alpha_0^3 + \frac{0.66}{1-\alpha_0^2} \tag{2}$$

The initial compliance value is computed for each test by applying the least squares method. Such an interpolation is performed by fitting the experimental data (in terms of load against CMOD) with a line, aiming to maximise the coefficient of

determination in a range of CMOD from 0.00 to 0.01mm. The same procedure is followed to determine the final compliance.

Under mixed mode loading, the effective critical crack length $\underline{a} = a_0 + (a_1 + a_2)\cos\theta$ (Fig. 1) to determine the critical stress-intensity factor, $K^S_{(I+II)C}$, is obtained from the following equation [51]:

$$E = \frac{6S}{C_u W^2 B} a_0 \left\{ V\left(\frac{a_0}{W}\right) + \right.$$
$$+ \left[\cos^6\frac{\theta}{2} + \sin^2\frac{\theta}{2}\cos^4\frac{\theta}{2}\right]\left[(a_0 + a_1\cos\theta)V\left(\frac{a_0 + a_1\cos\theta}{W}\right) - a_0 V\left(\frac{a_0}{W}\right)\right] + \quad (3)$$
$$\left. + \left[\cos^3\theta + \sin^2\theta\cos\theta\right]\left[(a_0 + a_1\cos\theta + a_2\cos\theta)V\left(\frac{a_0 + a_1\cos\theta + a_2\cos\theta}{W}\right) - (a_0 + a_1\cos\theta)V\left(\frac{a_0 + a_1\cos\theta}{W}\right)\right]\right\}$$

where $a_1 = 0.3\,a_0$, C_u is the unloading compliance (Fig. 2), $V(\alpha)$ is deduced from Eq.(2) by replacing α_0 with $\alpha = \underline{a}/W$, and a_2 is an unknown quantity which can be computed from Eq.(3) through an iterative procedure. Note that Eq.(3) was obtained by employing both the Castigliano theorem and the analytical solutions for the SIFs of a bent crack [53,54].

As is shown in Figure 1, the kinked crack branch consists of two segments, named a_1 and a_2. If the value of a_2 obtained from Eq.(3) is negative, it means that the effective crack length is $\underline{a} = a_0 + a_1$, with $a_1 \le 0.3\,a_0$. In this case, the effective critical crack length $\underline{a}$ (Fig. 1) to determine the critical stress-intensity factor, $K^S_{(I+II)C}$, is obtained from the following equation:

$$E = \frac{6S}{C_u W^2 B}\left\{a_0 V\left(\frac{a_0}{W}\right) + \left[\cos^6\frac{\theta}{2} + \sin^2\frac{\theta}{2}\cos^4\frac{\theta}{2}\right]\left[(a_0 + a_1\cos\theta)V\left(\frac{a_0 + a_1\cos\theta}{W}\right) - a_0 V\left(\frac{a_0}{W}\right)\right]\right\} \quad (4)$$

Note that, in the case of kinking angle θ equal to zero, Eqs(3) and (4) correspond to the unique equation provided by the TPFM [12].

Finally, the critical stress-intensity factor, $K^S_{(I+II)C}$, is computed by employing the measured value of the peak load, $P_{\max}$, and considering a straight crack having length equal to the projected length of the effective kinked crack [52]:

$$K^S_{(I+II)C} = \frac{3P_{\max}}{2W^2 B}\sqrt{\pi\left[a_0 + (a_1 + a_2)\cos\theta\right]}\, f(\alpha) \quad \text{with:} \quad \alpha = \frac{a_0 + (a_1 + a_2)\cos\theta}{W} \quad \text{when} \quad a_1 = 0.3\,a_0 \qquad (5)$$

or

$$K^S_{(I+II)C} = \frac{3P_{\max}}{2W^2 B}\sqrt{\pi\left[a_0 + a_1\cos\theta\right]}\, f(\alpha) \quad \text{with:} \quad \alpha = \frac{a_0 + a_1\cos\theta}{W} \quad \text{when} \quad a_1 < 0.3\,a_0 \qquad (6)$$

where function $f(\alpha)$ is given by:

$$f(\alpha) = \frac{1}{\sqrt{\pi}}\,\frac{1.99 - \alpha(1-\alpha)(2.15 - 3.93\alpha + 2.70\alpha^2)}{(1+2\alpha)(1-\alpha)^{3/2}} \qquad (7)$$

3. MTPM APPLICATION TO FRC SPECIMENS

Specimens are tested under three-point bending (Figure 1). Testing is performed by means of an Instron 8862 testing machine under crack mouth opening displacement (CMOD) control, employing a clip gauge at an average speed equal to 0.1 mmh^{-1}. All specimens exhibit a non-linear slow crack growth before the peak load is reached.

Each specimen consists of a beam 40mm x 40mm x 200mm (S=160mm), and presents a notch of 13.3mm in the lower part of the middle cross-section. Note that the depth (W) is taken equal to the width

(B) of the specimen, having previously verified that the B size will not influence the fracture behaviour of FRC specimen.

The specimen matrix is cementitious and characterised by the following proportions: cement: water: aggregates (by weight) = 1: 0.7 : 3.6. The maximum aggregate size is 4mm, and the cement is a 42.5 CEM II/A-P. This mixture presents a compressive strength of 30MPa at 28 days.

Three types of specimens are tested: plain concrete specimens (from P-1 to P-4 in Table 1), concrete specimens reinforced by randomly-distributed micro-synthetic polypropylene fibrillated fibres with a content equal to 0.5% by volume (from R05-1 to R05-4 in Table 1) or 2.5% by volume (from R25-1 to R25-4 in Table 1).

Such fibres (named Micrograminflex) are produced by LA MATASSINA GROUP (Vicenza- Italy), a Company leader in the production of fibres for concrete reinforcement [55]. Such micro-fibres are deformed and/or irregular (fibrillated) in shape, and made of 100% pure high-density polypropylene. The fibre aspect ratio is equal to 0.003 (fibre length equal to 18mm). The tensile strength and the elastic modulus are equal to 450-600MPa and 3.5kN/mm^2, respectively. Such fibres are generally used for secondary concrete reinforcement and cement mix shrinkage control.

4. RESULTS AND DISCUSSION

The fracture toughness $K^S_{(I+II)C}$ is computed for each specimen according to Eq. (5) or (6), by employing the corresponding load-

CMOD curve. The load – CMOD plot for specimen R05-1 is shown in Figure 2. The $K^S_{(I+II)C}$ values are listed in Table 1. Further, the values of $K^S_{(I)C}$ according to the TPFM are also computed (by assuming $\theta = 0$) and listed in last column of Table 1.

Table 1

The elastic modulus E, the kinking angle θ (Fig.1), the peak load $P_{\max}$, and the effective critical crack length $\underline{a}$ are also displayed in Table 1 for each tested specimen.

Note that crack generally grows under mixed mode (Figs 3-5).

Figures 3, 4, 5

When the kinking angle θ is not constant along the crack path (see Figure 6), the orientation of the first deflected segment $i+1$ (with $i = 1,...,N$, where N is a positive integer) such that $l_{i+1} > l_i$ is taken into account to compute the fracture toughness. Further, when the fracture surface is not plane, the mean value of such an angle is determined averaging the values related to front (Figure 6a) and back side (Figure 6b) of the specimen.

Figures 6

An error index I_e (%), defined in order to measure the relative difference between $K^S_{(I+II)C}$ and K^S_{IC}, is evaluated as follows:

$$I_e = \frac{K^S_{(I+II)C} - K^S_{IC}}{K^S_{IC}} 100\% \quad (8)$$

The absolute value $|I_e|$ of the above index against the kinking angle θ is plotted in Figure 7 for each type of specimen. Such data are well interpolated by the following three equations (see the continuous lines in Fig.7), one for each specimen type:

$$\text{Type P:} \quad |I_e| = 0.0074737249 18\theta^2 - 0.030065270 34\theta + 0.1412416843 \quad (9a)$$

$$\text{Type R05:} \quad |I_e| = 0.0035577226 89\theta^2 + 0.088404887 74\theta + 0.1811664899 \quad (9b)$$

$$\text{Type R25:} \quad |I_e| = 0.0015904417 26\theta^2 + 0.161595418 1\theta - 0.3176363167 \quad (9c)$$

It can be observed that, for θ greater than about 30°, the application of TPFM instead of MTPM produces an overestimation of the fracture toughness value, which increases by decreasing the fibre content.

Figure 7

Then, the effect of fibre content is evaluated in terms of elastic modulus, peak load, and critical SIF under mixed mode stress state (Figure 8), by interpolating the averaged experimental values of the above parameters for three different values of fibre content (FC%). The following expressions are obtained:

$$E = 17905\, e^{(-0.02 \cdot FC\%)} \quad (10a)$$

$$P_{\max} = 684.44\, e^{(0.0434 FC\%)} \quad (10b)$$

$$K^S_{(I+II)C} = 0.517\, e^{(0.0982 \cdot FC\%)} \quad (10c)$$

Figure 8

Further, the single values related to the elastic modulus, peak load, and critical SIF under mixed mode stress state are shown in Figure 8.

For fibre content FC equal to 3%, the above equations estimate a decrease of E equal to about 6% and an increase of $P_{\max}$ and $K^{S}_{(I+II)C}$ equal to about 14% and 34%, with respect to the values related to plain concrete specimens.

5. EXPERIMENTAL EVALUATION OF FPZ

The value of the effective critical crack length is compared with that experimentally deduced through the field of longitudinal displacements. The Digital Image Correlation (DIC) technique is used to extract 2D full-field maps of experimental displacements in the mid-span zone of each specimen.

Specimens are irregularly spray-painted before testing in order to get a well-contrasted grey-scale speckle pattern. A full-format Nikon D3X (6048x4032 pixels) digital camera is employed for data acquisition. The camera captures images of the suitably illuminated specimen surface at a rate of one frame every 15 seconds for plain concrete specimens and every 30 sec for FRC specimens.

The sequence of images has been treated by means of the software Ncorr developed in MATLAB environment [56]. The horizontal relative displacements are analysed between two parallel reference vertical lines symmetrically located with respect to the mid-span section, when the peak load is achieved. By examining, for example, the

contour plot of the horizontal displacements for specimen R25-3 shown in Figure 9, a discontinuity of such displacements ahead of the initial notch length can be observed, indicating a stable propagation of the crack prior to failure.

Figure 9

In Figures (10)-(12), the horizontal relative displacements determined through the DIC technique at the mid-span cross-section are displayed against the x-coordinate (shown in Fig. 1), for each tested specimen. The experimental displacement profile is plotted in thick line.

Figures 10, 11, 12

By interpolating with a thin line the experimental displacement values related to the notch depth zone (x from 0.0 to a_0), the value of x for which such a line deviates from the experimental displacement profile represents the experimental value of the effective critical crack length.

It can be observed that the experimental values of $\underline{a}$ (from Figs (10)-(12)) are in quite satisfactory agreement with the analytical ones, listed in Table 1 and represented by the horizontal dashed lines in Figs (10)-(12).

6. CONCLUSIONS

In the present paper, the fracture behaviour of FRC specimens, characterized by micro-synthetic polypropylene fibrillated fibres randomly distributed in the cementitious matrix, has been examined. The modified two-parameter model has been employed in order to take into account the possible crack deflection (kinked crack) during stable crack propagation.

Three types of specimens have been analysed: (a) plain concrete specimens, (b) concrete specimens with fibre content equal to 0.5% by volume or (c) fibre content equal to 2.5% by volume.

The concrete fracture toughness has been observed to improve by increasing the volume fraction of fibres, and an equation has been proposed to estimate such a parameter for a given fibre content. The overestimation of the fracture toughness determined by considering crack propagation under pure Mode I loading has been also evaluated, and an equation has been proposed to compute such an increment for a given kinking angle value.

Acknowledgements

The authors gratefully acknowledge the financial support provided by the Italian Ministry for University and Technological and Scientific Research (MIUR), Research Grant PRIN 2015 No. 2015JW9NJT on "Advanced mechanical modeling of new materials and structures for the solution of 2020 Horizon challenges".

References

[1] Y. Wang, Toughness characteristics of synthetic fibre-reinforced cementitious composites, Fatigue Fract. Engng. Mater. Struct. 21 (1998) 521-32.
[2] G. Appa Rao, A.S. Rao, Toughness indices of fiber reinforced concrete subjected to mode II loading, in: B.H. Oh et al. (Eds.), Fracture Mechanics of Concrete and Concrete Structures - Recent Advances in Fracture Mechanics of Concrete, Seoul, 2010, pp. 112-117.
[3] S. Xu, X Zhang, Determination of fracture parameters for crack propagation in concrete using an energy approach, Engng Fract. Mech. 75 (2008) 4292-308.
[4] Z.P. Bazant, Concrete fracture models: testing and practice, Engng Fract. Mech. 69 (2002) 165-205.
[5] D.S. Dugdale, Yielding of Steel Sheets Containing Slits, J. Mechanics, Physics and Solids 8 (1960) 100-04.
[6] G.J. Barenblatt, The Mathematical Theory of Equilibrium Crack in the Brittle Fracture, Advance in Applied Mechanics 7 (1962) 55-125.
[7] A.A. Griffith, The Phenomenon of Rupture and Flow in Solids, Philosophical Transactions of Royal Society of London A221 (1921) 163-197.
[8] S. Kumar, S.V. Barai, Determining the double-K fracture parameters for three-point bending notched concrete beams using weight function, Engng Fract. Mech. 76 (2009) 935-48.
[9] M.F. Kaplan. Crack propagation and the fracture of concrete. J. Am. Concr. Inst. 58 (1961) 591–610.
[10] A. Hillerborg, M. Modeer, P.E. Petersson, Analysis of crack formation and crack growth in concrete by means of fracture mechanics and finite elements. Cem. Concr. Res. 6 (1976) 773–82.
[11] Z.P. Bazant, B.H. Oh, Crack band theory for fracture of concrete. Mater. Struct. 16 (1983) 155–77.
[12] Y.S. Jenq, S.P. Shah, Two parameter fracture model for concrete. J. Engng Mech., ASCE 1985 111 (1985) 1227–41.
[13] Z.P. Bazant, J.-K. Kim, P.A. Pfeiffer, Determination of fracture energy from size effect and brittleness number. ACI Mater J. 84 (1987) 463–80.
[14] Z.P. Bazant, M.T. Kazemi, Determination of fracture energy, process zone length and brittleness number from size effect, with application to rock and concrete. Int J Fract 44 (1990) 111–31.
[15] S.E. Swartz, C.G. Go, Validity of compliance calibration to cracked concrete beams in bending. Exp. Mech. 24 (1984) 129–34.
[16] P. Nallathambi, B.L. Karihaloo, Determination of specimen-size independent fracture toughness of plain concrete. Mag. Concr. Res. 38 (1986) 67–76.
[17] S.E. Swartz, T.M.E Refai, Influence of size on opening mode fracture parameters for precracked concrete beams in bending, in: S.P. Shah, S.E. Swartz (Eds.), Fracture of Concrete and Rock, Houston, Texas, 1987, pp. 242-54.
[18] B.L. Karihaloo, P. Nallathambi, Effective crack model for the determination of fracture toughness of concrete. Engng Fract. Mech. 35 (1990) 637–45.

[19] S. Xu, H.W. Reinhardt, Determination of double-K criterion for crack propagation on quasi-brittle fracture, part I: experimental investigation of crack propagation. Int. J. Fract. 98 (1999) 111–49.
[20] S. Xu, H.W. Reinhardt, Determination of double-K criterion for crack propagation on quasi-brittle fracture, part II: analytical evaluating and practical measuring methods for three-point bending notched beams. Int. J. Fract. 98 (1999) 151–77.
[21] S. Xu, H.W. Reinhardt, Determination of double-K criterion for crack propagation on quasi-brittle fracture, part III: compact tension specimens and wedge-splitting specimens. Int. J. Fract. 98 (1999) 179–93.
[22] S. Xu, H.W. Reinhardt, A simplified method for determining double-K fracture parameters for three-point bending tests. Int. J. Fract. 104 (2000) 181–208.
[23] A. Caporale, L. Feo, R. Luciano ,Damage mechanics of cement concrete modeled as a four-phase composite, Composites Part B: Engineering 65 (2014) 124-30.
[24] L. Feo, F. Greco, L. Leonetti, R. Luciano, Mixed-mode fracture in lightweight aggregate concrete by using a moving mesh approach within a multiscale framework, Composite Structures 123 (2015) 88-97.
[25] M. Di Paola, M.F. Granata, Fractional model of concrete hereditary viscoelastic behaviour, Archive of Applied Mech. (2016), DOI: 10.1007/s00419-016-1196-7, in press.
[26] Z.P. Bazant, M.T. Kazemi, Size dependency of concrete fracture energy determined by RILEM work-of-fracture method. Report No 89-12/B623s, Northwestern University, Evanston, 1989.
[27] RILEM Technical Committee 89-FMT. Determination of fracture parameters (KsIC and CTODc) of plain concrete using tree-point bend tests, proposed RILEM draft recommendations. Mater. Struct. 23 (1990) 457–60.
[28] RILEM Technical Committee 89-FMT, Size-effect method for determining fracture energy and process zone size of concrete, proposed RILEM draft recommendations. Mater. Struct. 23 (1990) 461–65.
[29] Y.S. Jenq, Al. Carpinteri, Fracture mechanics test methods for concrete. Report of Technical Committee 89-FMT fracture mechanics of concrete: test methods RILEM. Chapman Hall, London, 1991.
[30] RILEM draft recommendation (50-FMC), Determination of the fracture energy of mortar and concrete by means of three-point bend test on notched beams. Mater. Struct. 18 (1985) 285–90.
[31] I. de Freitas, F. Darwish, M. V. Pereira, K. Allende, Fracture behaviour of polymeric fiber reinforced lightweight structural concrete, Materials Research 17 (2014) 1588-93.
[32] A. Sivakumar, M. Santhanam, Mechanical properties of high strength concrete reinforced with metallic and non-metallic fibers. Cement and Concrete Composites 29 (2007) 603-08.
[33] V.S. Gopalaratnam, S.P. Shah, G. Batson, M. Criswell, V. Ramakishnan, M. Wecharatana, Fracture Toughness of Fiber Reinforced Concrete, Materials Journal 88 (1991) 339-53.
[34] ACI Committee 544, State-of-the-art Report on Fiber Reinforced Concrete, 544.1R-82 (reapproved 1986), American Concrete Institute, Detroit (1986).

[35] J.G. Keer, Fiber reinforced concrete, in: (R.N. Swamy, Ed.), New Reinforced Concretes: Concrete Technology and Design Vol.2, Surrey University Press, 1984, pp.2–105.
[36] A. Bentur and S. Mindess, Fiber Reinforced Cementititous Composites, Elsevier, London, 1990.
[37] Y. Wang, S. Backer, V.C. Li, An experimental study of synthetic fiber reinforced cementitious composites. J. Mater. Sci. 22 (1987) 4281–91.
[38] V.S. Gopalaratnam, R. Gettu, On the characterization of flexural toughness in fiber reinforced concretes, Cement and concrete composites 17 (1995) 239-54.
[39] V.S. Gopalaratnam, R. Gettu, S. Carmona, D. Jamet, Characterization of the toughness of fiber reinforced concretes using the load-CMOD response, in: (F.H. Wittmann Ed.) Proceedings FRAMCOS2, AEDIFICATIO Publishers, Freiburg, 1995, pp. 769-82.
[40] A. Carpinteri, A. Spagnoli, S. Vantadori, A fracture mechanics model for a composite beam with multiple reinforcements under cyclic bending. Int. J. Solids and Struct. 41 (2004) 5499-515.
[41] A. Carpinteri, A. Spagnoli, S. Vantadori, Mechanical damage of ordinary or prestressed reinforced concrete beams under cyclic bending. Engng Fract. Mech. 72 (2005) 1313-28.
[42] A. Carpinteri, A. Spagnoli, S. Vantadori, An elastic-plastic crack bridging model for brittle-matrix fibrous composite beams under cyclic loading. Int. J. Solids and Struct. 43 (2006) 4917-36.
[43] L-P. Guo, A. Carpinteri, R. Roncella, A. Spagnoli, W. Sun, S. Vantadori, Fatigue damage of high performance concrete through a 2D mesoscopic lattice model. Computat. Mat. Sc. 44 (2009) 1098-106.
[44] O.B. Ozger, F. Girardi, G.M. Giannuzzi, V.A. Salomoni, C.E. Majorana, L. Fambri, N. Baldassino, R. Di Maggio, Effect of nylon fibres on mechanical and thermal properties of hardened concrete for energy storage systems, Mat. and Design 51 (2013) 989-97.
[45] G. Mazzucco, C.E. Majorana, V.A. Salomoni, Numerical simulation of polypropylene fibres in concrete materials under fire conditions Comput. and Struct. 154 (2015) 17-28.
[46] S.-W. Kim, W.-S. Park, Y.-I. Jang, L. Feo, , H.-D.Yun, Crack damage mitigation and shear behavior of shear-dominant reinforced concrete beams repaired with strain-hardening cement-based composite, Composites Part B: Engng 79 (2015) 6-19.
[47] A. Hillerborg, Analysis of one single crack, in: (F.H. Wittmann Ed.) Fracture Mechanics of Concrete, Elsevier Science, London, 1983, pp. 223-49.
[48] A. Hillerborg, Determination and significance of the fracture toughness of steel fibre concrete, in: (S.P. Shah, A. Skarendahl Eds) Steel Fiber Concrete, Elsevier Science, London, 1985, pp. 257-71.
[49] V.C. Li, H. Stang, H. Krenchel. Micromechanics of crack bridging in fibre-reinforced concrete. Mater. Struct. 26 (1993) 486-94.
[50] L. Bryars, R. Gettu, B. Barr, A. Ariño, Size effect in the fracture of fiber-reinforced high-strength concrete, in: Fracture and damage in quasi-brittle structures, E&FN Spon, London, 1994, pp. 319–326.

[51] A. Carpinteri, F. Berto, G. Fortese, C. Ronchei, D. Scorza, S. Vantadori, Modified two-parameter fracture model for bone, in press, http://dx.doi.org/10.1016/j.engfracmech.2016.11.002.
[52] H. Tada, P.C. Paris, G.R. Irwin. The Stress Analysis of Cracks Handbook. 3rd Ed, ASME Press, New York, 2000.
[53] H. Kitagawa, R. Yuuki, T. Ohira, Crack-morphological aspects in fracture mechanics, Engng Fract. Mech. 7 (1975) 515–29.
[54] B. Cotterell, J.R. Rice, Slightly curved or kinked cracks. Int. J. Fracture 16 (1980) 155-69.
[55] http://www.lamatassina.it/
[56] http://www.ncorr.com/

Special issue on Mixed Mode Fracture
Theoretical and Applied Fracture Mechanics – January 2017
REVISED VERSION - February 2017

Mode I fracture toughness of fibre reinforced concrete

Andrea CARPINTERI, Giovanni Fortese, Camilla RONCHEI, Daniela SCORZA, Sabrina VANTADORI

Dept. of Engineering and Architecture,
University of Parma, Parco Area delle Scienze 181/A, 43124 Parma, Italy
Corresponding Author: Sabrina Vantadori sabrina.vantadori@unipr.it

LIST OF FIGURES AND TABLES CAPTIONS

Figure 1. Crack propagation under mixed mode stress state: specimen geometry and applied loading.

Figure 2. Load – CMOD plot for specimen R05-1.

Table 1. Elastic modulus E, critical SIF $K^{S}_{(I+II)C}$ under mixed stress state, crack kinking angle θ, peak load $P_{\max}$, effective critical crack length $\underline{a}$, critical SIF K^{S}_{IC} under Mode I loading, and error index modulus, $|I_e|$.

Figure 3. Front side and back side of the fractured zone in plain concrete specimens: (a)-(b) P-1; (c)-(d) P-2; (e)-(f) P-3; (g)-(h) P-4.

Figure 4. Front and back side of the fractured zone in fibre reinforced concrete specimens with a fibre content equal to 0.5% by volume: (a)-(b) R05-1; (c)-(d) R05-2; (e)-(f) R05-3; (g)-(h) R05-4.

Figure 5. Front and back side of the fractured zone in fibre reinforced concrete specimens with a fibre content equal to 2.5% by volume: (a)-(b) R25-1; (c)-(d) R25-2; (e)-(f) R25-3; (g)-(h) R25-4.

Figure 6. Procedure used in order to measure θ. Specimen R05-1 is shown: (a) front side; (b) back side.

Figure 7. Absolute value $|I_e|$ of the error index against the kinking angle θ, for three values of the fibre content.

Figure 8. Fibre content effect on: (a) elastic modulus E, (b) peak load $P_{\max}$, and (c) critical SIF $K^{S}_{(I+II)C}$ under mixed mode stress state.

Figure 9. Contour plot of the horizontal displacements for specimen R25-3 when the peak load is achieved. Displacements in mm.

Figure 10. Longitudinal displacements determined employing the Digital Image Correlation technique (DIC) for the following specimens: (a) to (d) P-1 to P-4. Displacements in the notch zone are in grey.

Figure 11. Longitudinal displacements determined employing the Digital Image Correlation technique (DIC) for the following specimens: (a) to (d) R05-1 to R05-4. Displacements in the notch zone are in grey.

Figure 12. Longitudinal displacements determined employing the Digital Image Correlation technique (DIC) for the following specimens: (a) to (d) R25-1 to R25-4. Displacements in the notch zone are in grey.

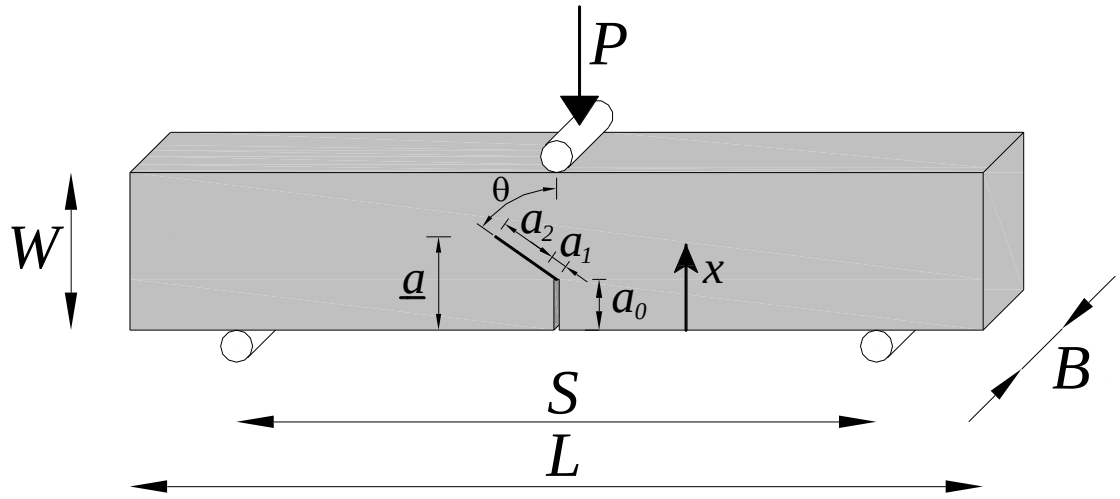

Figure 1.

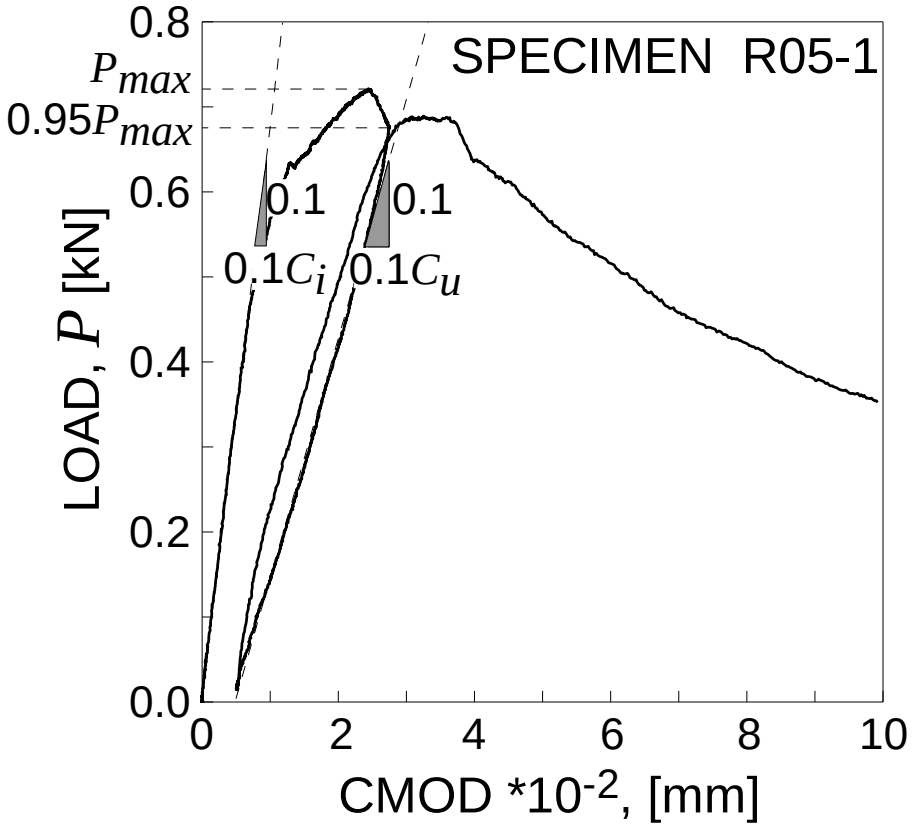

Figure 2.

Table 1.

Specimen No.	E [MPa]	$K^{S}_{(I+II)C}$ [MPa m$^{1/2}$]	θ [°]	$P_{\max}$ [N]	$\underline{a}$ [mm]	K^{S}_{IC} [MPa m$^{1/2}$]	$\lvert I_e \rvert$ [%]
P-1	17990.97	0.529	11.0	575.972	17.56	0.534	1
P-2	17949.34	0.509	47.5	674.510	18.26	0.605	16
P-3	17923.74	0.465	40.5	745.785	20.43	0.521	11
P-4	17945.35	0.535	20.5	635.751	19.04	0.550	3
R05-1	17514.85	0.570	20.0	721.486	19.00	0.587	3
R05-2	17672.37	0.548	0.0	858.498	16.34	0.548	0
R05-3	17928.08	0.544	10.0	697.524	16.95	0.555	2
R05-4	17474.96	0.550	30.0	661.493	18.97	0.586	6
R25-1	17014.18	0.688	63.0	797.779	23.24	0.818	16
R25-2	17068.80	0.622	20.0	763.130	19.40	0.639	3
R25-3	16862.08	0.664	25.5	743.270	18.58	0.696	5
R25-4	16838.15	0.659	38.0	717.562	19.87	0.726	9

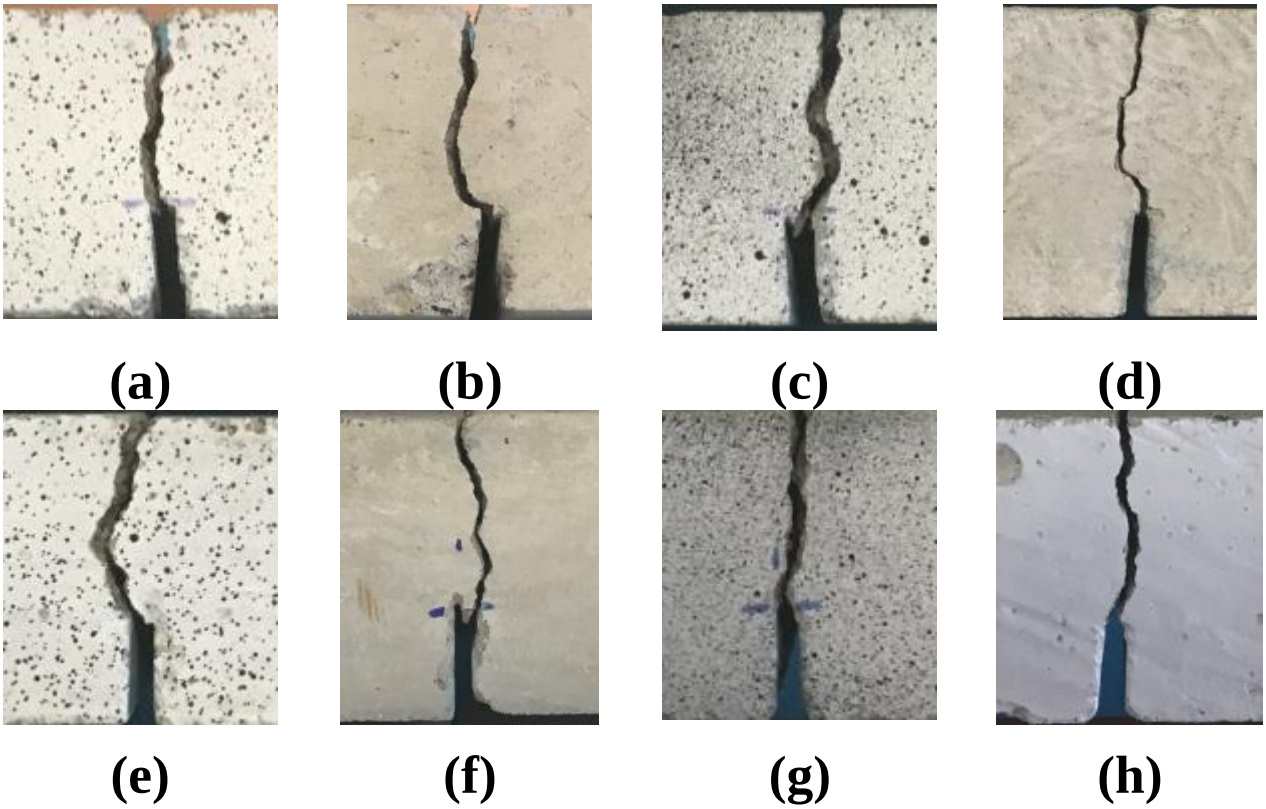

Figure 3.

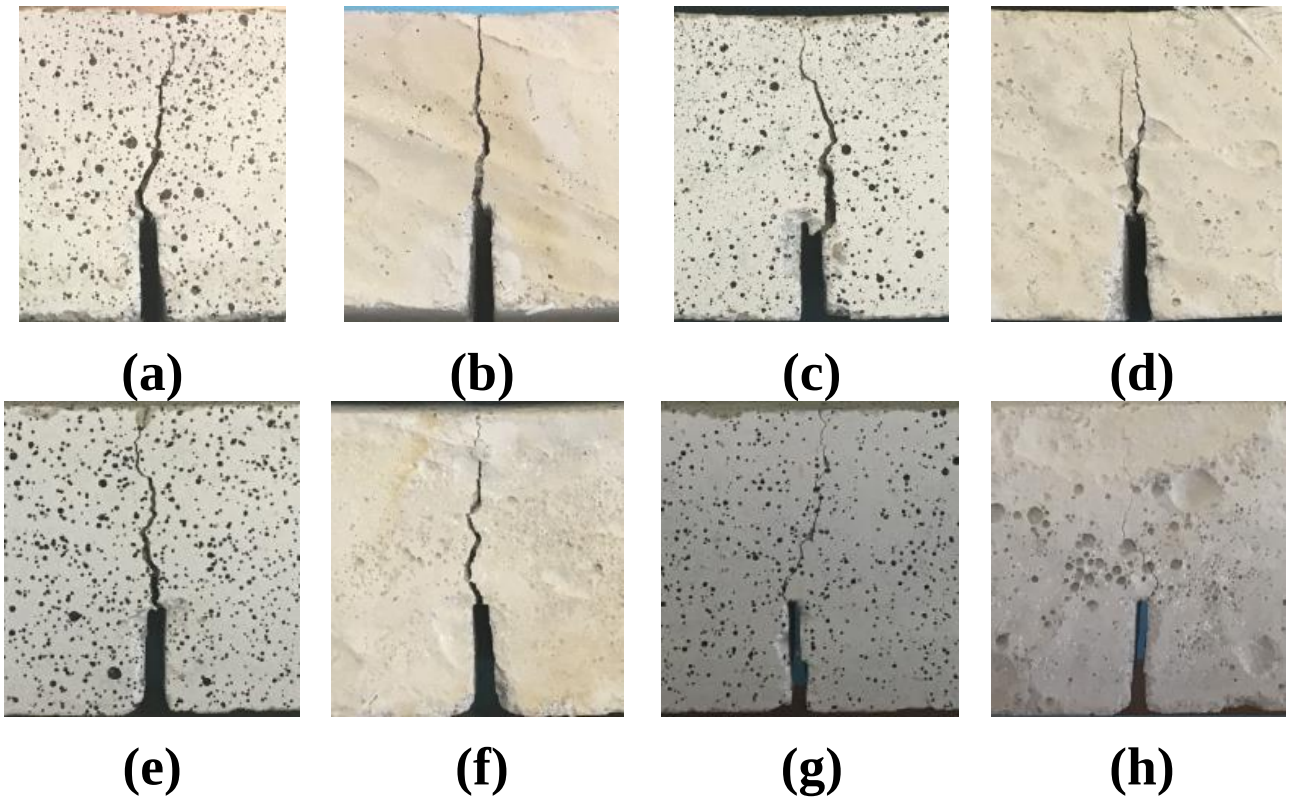

Figure 4.

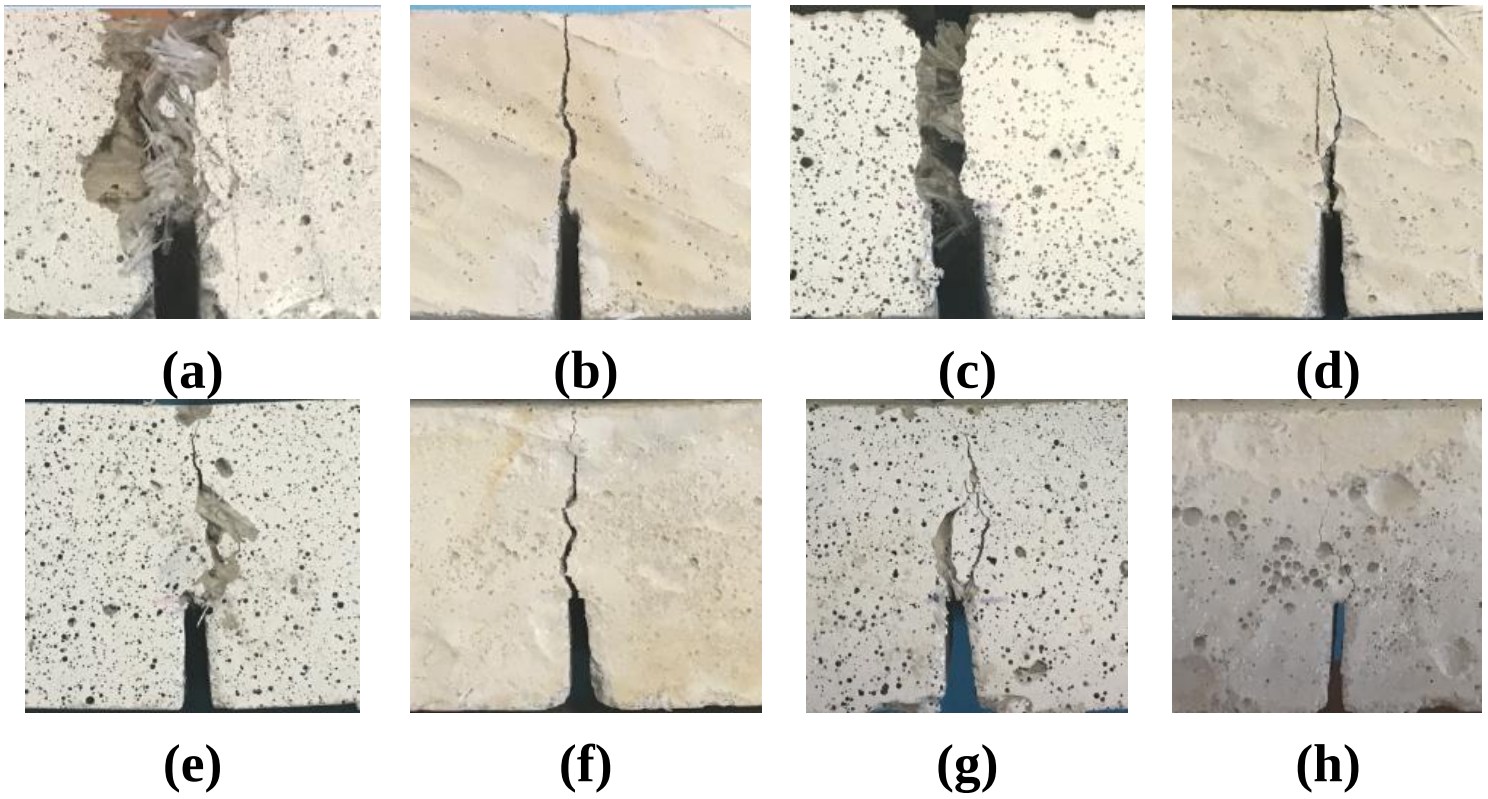

Figure 5.

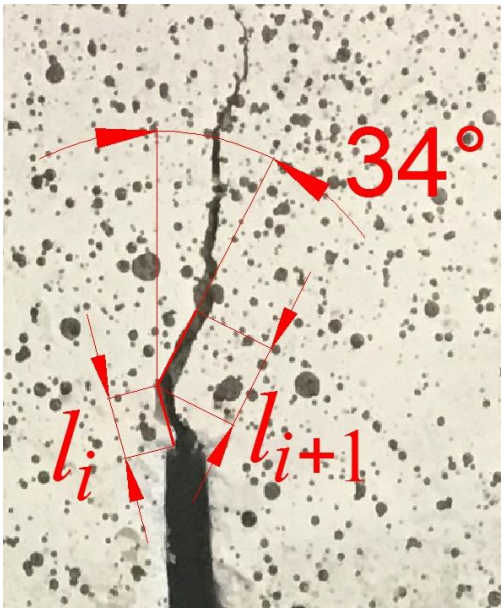

(a)

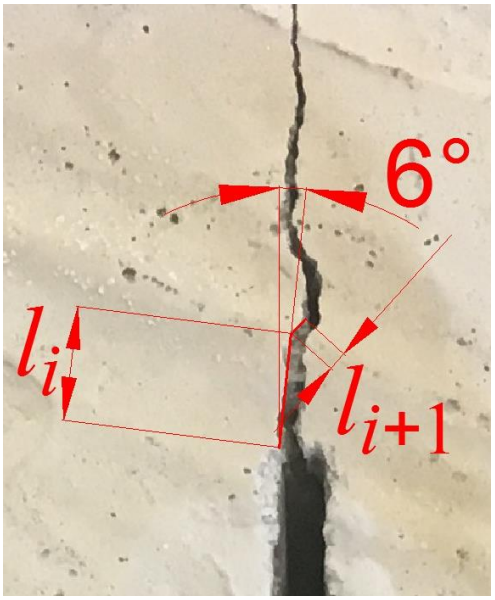

(b)

Figure 6.

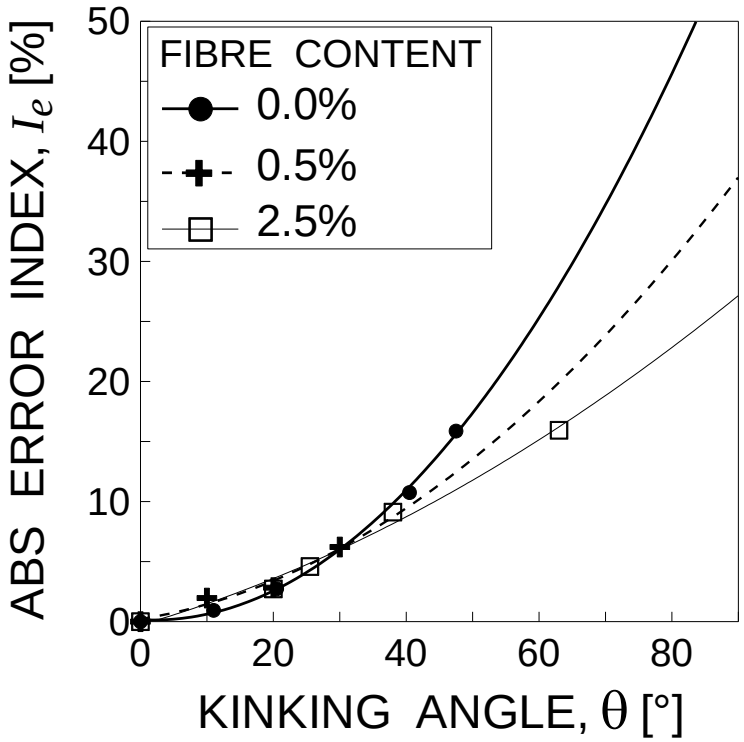
FIBRE CONTENT
0.0%
0.5%
2.5%
ABS ERROR INDEX, I_e [%]
KINKING ANGLE, θ [°]
0
10
20
30
40
50
0
20
40
60
80

Figure 7.

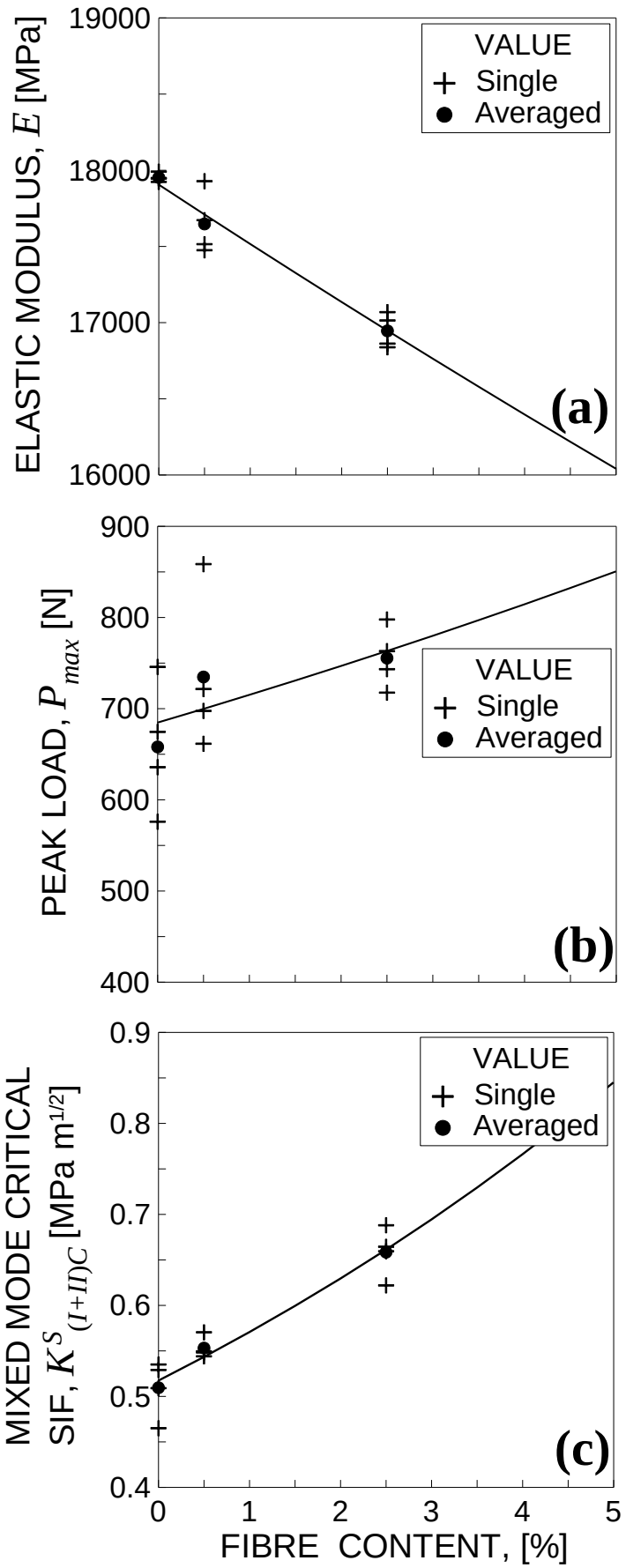
ELASTIC MODULUS, E [MPa]
19000
18000
17000
16000
VALUE
Single
Averaged
(a)
PEAK LOAD, P max [N]
900
800
700
600
500
400
VALUE
Single
Averaged
(b)
MIXED MODE CRITICAL SIF, K S (I+II)C [MPa m1/2]
0.9
0.8
0.7
0.6
0.5
0.4
VALUE
Single
Averaged
(c)
0
1
2
3
4
5
FIBRE CONTENT, [%]

Figure 8.

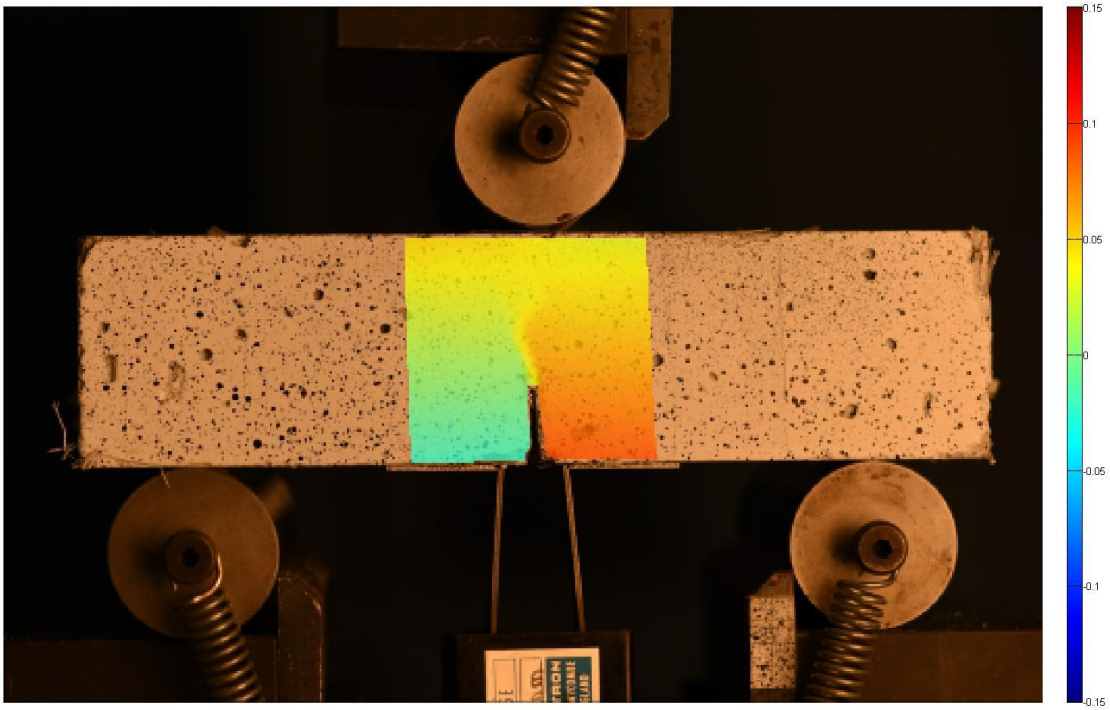

Figure 9.

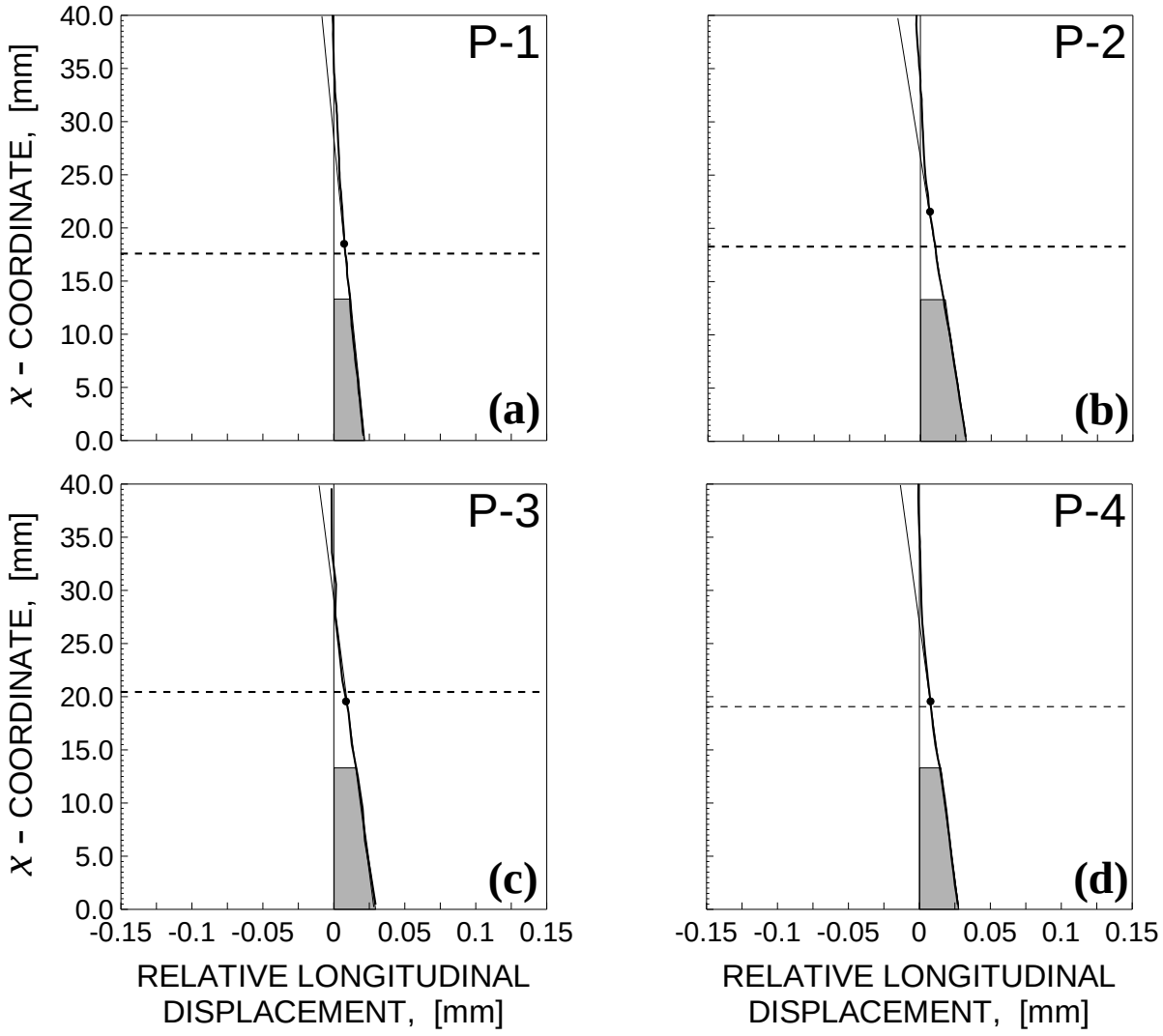
P-1
P-2
P-3
P-4
(a)
(b)
(c)
(d)
X - COORDINATE, [mm]
40.0
35.0
30.0
25.0
20.0
15.0
10.0
5.0
0.0
-0.15 -0.1 -0.05 0 0.05 0.1 0.15
RELATIVE LONGITUDINAL DISPLACEMENT, [mm]

Figure 10.

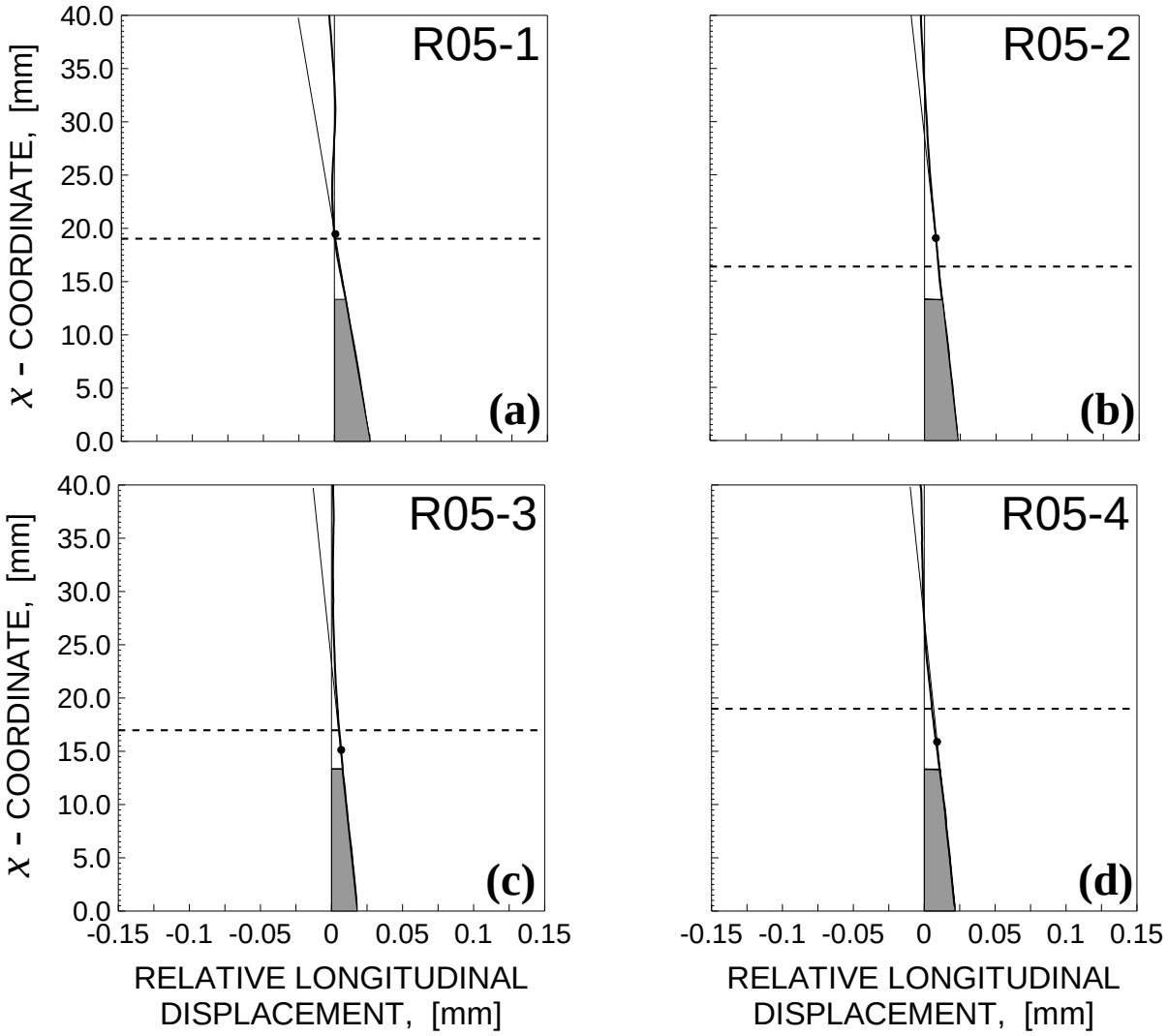
R05-1
R05-2
R05-3
R05-4
(a)
(b)
(c)
(d)
χ - COORDINATE, [mm]
RELATIVE LONGITUDINAL DISPLACEMENT, [mm]
40.0
35.0
30.0
25.0
20.0
15.0
10.0
5.0
0.0
-0.15 -0.1 -0.05 0 0.05 0.1 0.15

Figure 11.

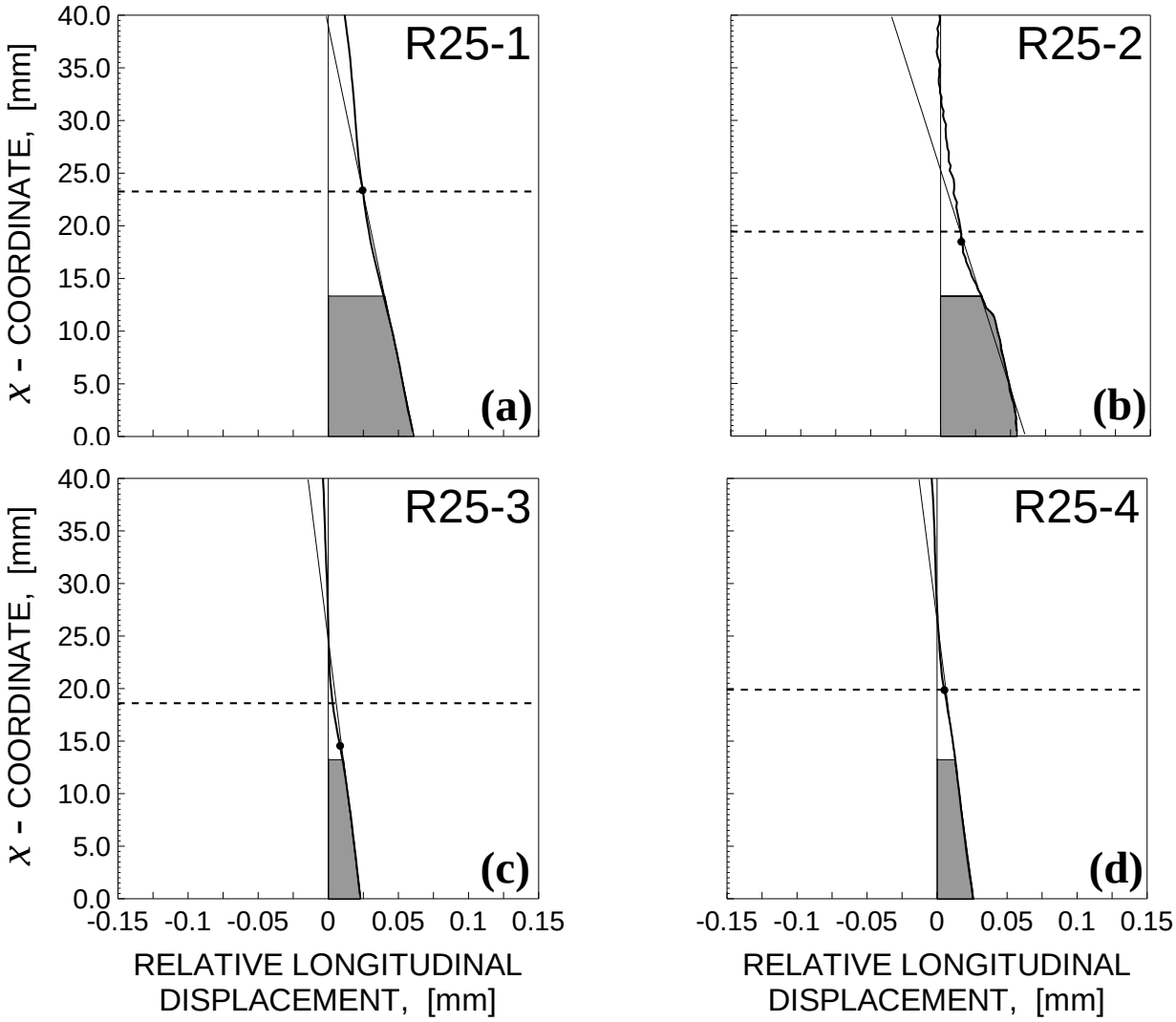
R25-1
R25-2
R25-3
R25-4
(a)
(b)
(c)
(d)
χ - COORDINATE, [mm]
40.0
35.0
30.0
25.0
20.0
15.0
10.0
5.0
0.0
-0.15 -0.1 -0.05 0 0.05 0.1 0.15
RELATIVE LONGITUDINAL DISPLACEMENT, [mm]

Figure 12.